Observation of Electron Shakeup in CdSe/CdS Core/Shell Nanoplatelets

Felipe V. Antolinez, Freddy T. Rabouw,[†] Aurelio A. Rossinelli, Jian Cui,[‡] and David J. Norris*

Optical Materials Engineering Laboratory, Department of Mechanical and Process Engineering, ETH Zurich, 8092 Zurich, Switzerland

S *Supporting Information*

ABSTRACT: While ensembles of CdSe nanoplatelets (NPLs) show remarkably narrow photoluminescence line widths at room temperature, adding a CdS shell to increase their fluorescence efficiency and photostability causes line width broadening. Moreover, ensemble emission spectra of CdSe/CdS core/shell NPLs become strongly asymmetric at cryogenic temperatures. If the origin of these effects were understood, this could potentially lead to stable core/shell NPLs with narrower emission, which would be advantageous for applications. To move in this direction, we report time-resolved emission spectra of individual CdSe/CdS core/shell NPLs at 4 K. We observe surprisingly complex emission spectra that contain multiple spectrally narrow emission features that change during the experiment. With machine-learning algorithms, we can extract characteristic peak energy differences in these spectra. We show that they are consistent with electron "shakeup lines" from negatively charged trions. In this process, an electron−hole pair recombines radiatively but gives part of its energy to the remaining electron by exciting it into a higher single-electron level. This "shakeup" mechanism is enabled in our NPLs due to strong exciton binding and weak lateral confinement of the charge carriers. Time-resolved single-photon-counting measurements and numerical calculations suggest that spectral jumps in the emission features originate from fluctuations in the confinement potential caused by microscopic structural changes on the NPL surface (e.g., due to mobile surface charges). Our results provide valuable insights into line width broadening mechanisms in colloidal NPLs.

KEYWORDS: *CdSe/CdS nanoplatelets, core/shell nanoplatelets, shakeup line, trion emission, weak confinement, machine learning*
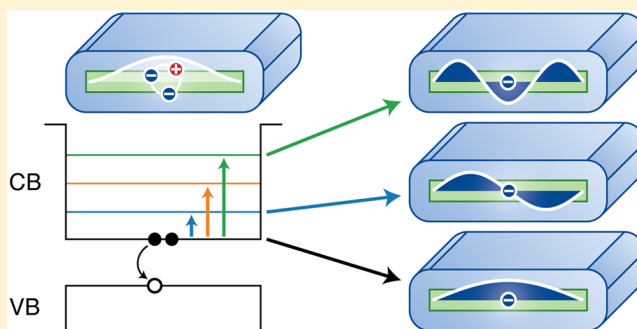
O ver the past decade, colloidal semiconductor nanocrystals with quasi-two-dimensional (2D) shapes have been introduced. Although this new class of nanomaterials includes semiconductor nanoribbons,[1] nanosheets,[2] and quantum belts,[3] arguably the most heavily studied system has been the semiconductor nanoplatelet (NPL).[4,5] NPLs consist of flat quasi-rectangular particles that have a uniform and atomically precise thickness. Amazingly, NPL samples can be synthesized in which all particles have the same thickness [e.g., 4 monolayers (MLs)]. Because this dimension determines the energy of photogenerated electron−hole pairs (or excitons), this uniformity results in extremely narrow fluorescence line widths (e.g., ∼35 meV for 4 ML CdSe NPLs).[6−8] Thus, compared to samples of quasi-spherical quantum dots, for which residual size distributions always broaden the emission spectra, NPLs provide better color purity for applications in displays, lighting, and lasers.

The underlying photophysical properties of NPLs are largely governed by the strong electron−hole interaction of the exciton. Due to the dielectric-confinement effect,[9] the exciton binding energy is large, and stable excitons and biexcitons exist at room temperature. This has implications for applications, e.g., in decreasing the threshold in lasers.[10−12] Unfortunately,

NPLs also suffer from significant nonradiative losses, as evidenced by their limited photoluminescence (PL) quantum efficiencies and strong fluorescence intermittency on the single-particle level.[13] Thus, applications relying on ensembles of NPLs typically suffer from poor fluorescence quantum yield (QY) and photostability.

A well-known strategy to enhance QY and photostability of semiconductor nanocrystals is to coat the active "core" material with a higher-bandgap semiconductor "shell," thereby protecting the photoexcited charge carriers from the environment and passivating surface defects.[14−16] To implement this approach in NPLs, procedures have been developed to overcoat CdSe NPLs with a CdS shell using colloidal atomic-layer deposition[17,18] or high-temperature continuous growth.[19] While the inorganic shell improves the QY and leads to more stable emission from individual NPLs, it also increases the room-temperature ensemble emission line width to ∼60 meV. The broadening of the emission line width has been attributed to increased phonon coupling.[19] However, the

ensemble line width remains broad and is strongly asymmetric even at cryogenic temperatures,[18] where phonon coupling should be suppressed. This observation has tentatively been attributed to inhomogeneities in composition, strain, surface passivation, or dimension[18] but could also originate from imperfect shells.

Here, we investigate the origin of the broad and asymmetric ensemble emission of CdSe/CdS core/shell NPLs at cryogenic temperatures using single-particle spectroscopy. We find that individual NPLs display emission spectra containing an unexpectedly complex series of narrow emission peaks, which change dramatically every few seconds. We use machine-learning algorithms to analyze large numbers of emission spectra efficiently and with minimal user input. Specifically, we rely on k-means clustering, an unsupervised machine-learning algorithm for pattern recognition, that has applications in many fields including computer vision[20] and biology.[21] Our machine-learning strategy allows for the reconstruction of high signal-to-noise spectra in addition to their corresponding decay dynamics. From our analysis, we attribute the observed emission peaks to a negative trion (a three-particle state with two electrons and one hole). The complex series of emission features is then consistent with a shakeup process, whereby the trion decays radiatively by electron−hole recombination to one of several possible excited states of the remaining electron. We propose that spontaneous fluctuations of the electrostatic potential in the NPL, for example, due to mobile surface defects or surface charges, change the coupling of the trion ground state to these different final single-electron states, leading to the strong and sudden spectral shifts that are observed.

For our experiments, we start with CdSe/CdS core/shell NPLs prepared according to a published protocol.[19] This synthesis yields NPLs that are roughly square in shape with a ~20 nm lateral size. The CdSe cores are 4 ML thick and are uniformly coated with ~12-ML-thick CdS shells. We deposited these particles on a Si chip with a 3 μm thick thermal-oxide layer (see section S1 in the Supporting Information). The sample was then mounted in a closed-cycle helium cryostat and measured under vacuum at a temperature of 4 K. Figure 1a shows the low-temperature photoluminescence (PL) spectrum recorded from an ensemble of NPLs (blue line) excited with a 405 nm laser (see Figure S1 and section S2 in the Supporting Information for details of the optical setup). The ensemble emission spectrum at 4 K is shifted to higher energy with respect to the room-temperature emission, as expected from lattice contraction. The pronounced tail on the low-energy side of the emission peak is also consistent with prior measurements on similar nanocrystals.[18] More surprisingly, the emission spectrum of a representative individual NPL with a 1 s exposure time (red line) features a series of sharp peaks.

To investigate further the emission behavior of individual NPLs, we recorded a series of emission spectra over 3 min. Each spectrum was collected with a 100 ms exposure time. Figure 1b shows the resulting spectral time series, representing a time-dependent emission spectrum for a single NPL that was excited with the 405 nm picosecond-pulsed laser. In these data, complete switching of the emission spectrum, including the positions and amplitudes of all emission peaks (e.g., at 42 s) is observed. In addition, the time series shows instances of simultaneous spectral diffusion of all emission peaks, for example, at 120 s. Interestingly, the total emission intensity as a function of time (Figure 1c) remains fairly steady (fluctuations
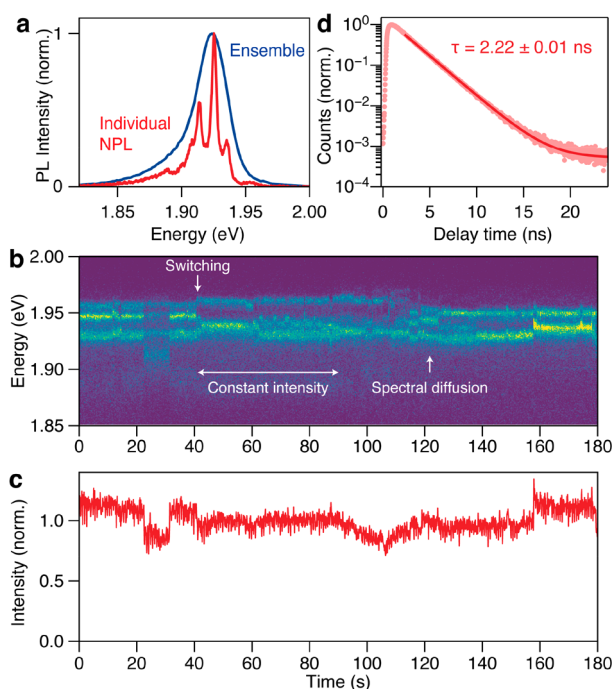

Figure 1. Photoluminescence from CdSe/CdS core/shell NPLs. (a) Emission spectrum (1 s exposure) of a representative individual (red line) CdSe/CdS core/shell NPL compared to the ensemble emission spectrum (blue line) at 4 K. (b) The emission spectrum from an individual NPL as a function of time, where each time frame is accumulated over 100 ms. Intensity is shown as a color scale in arbitrary units. (c) Total emission intensity of the time series shown in panel b. (d) Decay trace constructed by building a histogram from all photon arrival times recorded simultaneously with the time series in panel b. The resulting data can be fit well with a single-exponential lifetime of τ = 2.22 ns with a constant background level corresponding to 178 counts per second.

within 30%) while the emission spectra undergo these changes (such as in the time period between 42 and 90 s). This suggests that the sudden spectral shifts have a different origin than the commonly observed phenomenon of blinking of individual nanocrystals, which typically involves strong intensity fluctuations and is usually ascribed to spontaneous charging and discharging of the nanocrystal.[22]

By sending half of the photons to the spectrometer and half of the photons directly to an avalanche photodiode, we can record photon arrival times while collecting the spectral time series. Figure 1d shows the time-resolved PL decay histogram constructed from all photon arrival times recorded simultaneously with the data in Figure 1b,c. Fitting the resulting decay trace yields a single-exponential lifetime of τ = 2.22 ns. A constant background of 178 counts per second is responsible for <0.5% of the total photon counts. The extracted lifetime is significantly longer than the ~200 ps lifetime of CdSe core NPLs at cryogenic temperatures,[13,23] which can be ascribed to reduced electron−hole overlap because of electron delocalization in the CdS shell and weaker Coulomb interaction due to lower dielectric confinement. However, the lifetime that we measure is significantly shorter than the value of ~7 ns that has been measured for similar NPL heterostructures at T = 20 K.[18]

In single-nanocrystal experiments, time traces of the PL intensity are often used to assign particular emission intensity levels to different nanocrystal emission states.[24,25] In our case, this type of analysis is not possible because the emission
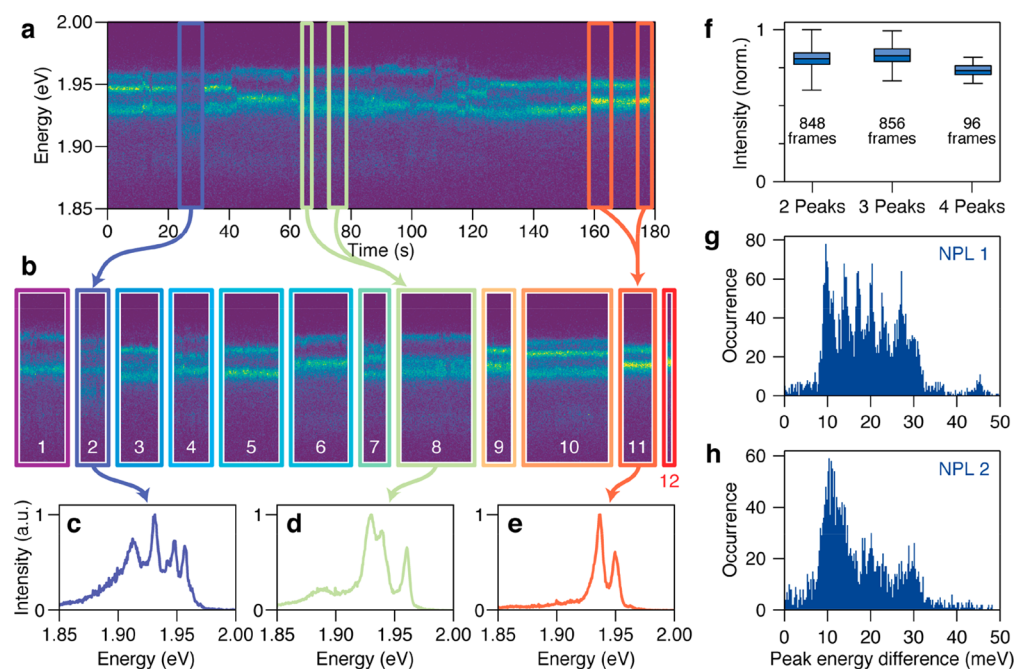
Figure 2. Spectral sorting with k-means clustering. (a) Same time-dependent emission spectra shown in Figure 1b. (b) With machine learning, the spectral time series in panel a can be sorted into a given number of emission clusters (color coded and numbered 1 through 12). (c)−(e) Average emission spectra for three of the clusters (2, 8, and 11) identified by machine learning. (f) Boxplot correlating the total emission intensity with the number of emission peaks per cluster. The horizontal line inside the box indicates the median value, the box extends from the lower to upper quartile values of the data, and the whiskers highlight the span of the data points. (g) Histogram of all peak energy differences observed in the data set from Figure 1b. (h) Histogram of observed peak energy differences for a different individual NPL (see Figure S2 in the Supporting Information for the corresponding spectral time series).

intensity fluctuates by only ∼30% (Figure 1c) even as the individual NPL is clearly undergoing changes in its emission spectrum. We therefore applied machine-learning algorithms to distinguish the emission states in the measured spectra for our NPLs with minimal user bias.[26] We employed a specific implementation of the k-means clustering algorithm[27] available in the Python programming language.[28] This allowed us to sort the 1800 individual frames shown in Figure 2a, where the number of clusters was the only user input. We arbitrarily chose 12 clusters, but as long as a sufficiently large number (>10) was chosen, very similar results were obtained. Each of the resulting 12 clusters in Figure 2b groups all spectral frames with similar emission spectra, even if they were not recorded consecutively. By averaging all frames within each cluster, spectra can be obtained for each cluster with a high signal-to-noise ratio (Figure 2c−e). In this particular data set, we observe that the NPL switches between states having two to four dominant emission features. While the averaged spectra from some clusters are quite distinct, groups of clusters exist that exhibit peaks that are only spectrally shifted but are otherwise very similar (e.g., clusters 5 and 6).

In general, several effects could explain why the PL spectrum displays multiple peaks: (1) emission from multiple nano-crystals in the focus (or multiple optically independent regions within the same particle[29]), (2) coupling to optical and acoustic phonons,[30] (3) simultaneous emission from several fine-structure states,[31] (4) rapid switching between different nanocrystal charge states,[30] and (5) biexciton cascade emission.[32] The last three possibilities would lead to multiexponential PL decay dynamics[33−37] and can therefore be excluded based on the data presented in Figure 1d. As we will now discuss in the next few paragraphs, two of the other

possibilities (multiple NPLs in focus and phonon coupling) can also be eliminated as the primary cause of the multiple emission peaks.

From just a single spectral frame, it is difficult to extract the number of observed emission peaks and their energy differences accurately. Therefore, we first use a peak-finding algorithm with minimal user input to count the number of peaks present in each frame based on the averaged emission spectrum of the corresponding cluster. Then, we fit each frame in the cluster separately with that particular number of Lorentzian peaks (see section S3 in the Supporting Information). Figure 2f shows the correlation between the total emission intensity and the number of emission peaks that are observed for a particular frame. We do not observe a positive correlation between the number of emission peaks and the overall intensity (if any, a negative correlation exists, which will be discussed later). Based on this, and the observation of simultaneous switching and spectral diffusion of all emission peaks in the spectral time series (Figure 1b), we exclude the possibility that the multiple emission peaks arise due to collection of signal from several independent NPLs.

Phonon coupling generally leads to one or several series of phonon replicas in single-particle PL spectra, with characteristic energy separations corresponding to the phonon modes involved. To check if particular peak energy separations occur frequently in our multipeaked spectra, we created a histogram of all peak energy separations observed in the data set. Figure 2g shows a histogram of the separations for the NPL described above (Figures 1 and 2a−e). The histogram in Figure 2h is constructed from the spectral time series of a different individual NPL on the same substrate (Figure S2 in the Supporting Information). While clearly some energy differ-

ences (particularly around 10 and 20 meV) appear more often than others, peak energy differences corresponding to the longitudinal-optical (LO) phonon at 25 meV for CdSe or 35 meV for CdS do not appear prominently. In contrast, when we repeat the analysis from Figure 2 on published data from an individual CdSe/CdS core/shell quantum dot[38] (see Figure S3 in the Supporting Information), we see clear evidence of peak energy differences related to the LO phonon. While a peak energy difference of 10 meV in the histogram of our CdSe/CdS core/shell NPL in Figure 2g could theoretically originate from the difference in LO-phonon energies between CdSe and CdS, the feature at 10 meV still occurs frequently in a histogram (see Figure S4 in the Supporting Information) constructed from only the peak energy differences with respect to the highest-energy peak (which would correspond to the zero-phonon line if the complex spectrum were due to phonon coupling). Therefore, we rule out optical phonon replicas as the origin of the multiple emission peaks observed for individual NPLs.

Experimental studies on spherical quantum dots of the same CdSe/CdS core/shell composition have shown that these nanocrystals can obtain permanent negative charge at cryogenic temperatures under vacuum, presumably due to photocharging.[24,31,39] Permanent charging can be caused by rapid and efficient hole localization on the CdS shell surface.[40−42] Previous experiments on CdSe/CdS NPLs have suggested that hole trapping on the surface can leave an electron that remains delocalized inside the NPL.[43] After eliminating the other possible explanations (1−5) for our multiple peaks, we propose that our NPLs are also negatively charged at cryogenic temperatures. This can then explain all of the observations in terms of emission from negative trions. Indeed, the nonblinking intensity trace (Figure 1c) and fast single-exponential decay behavior (Figure 1d) is consistent with emission from a bright trion ground state.[24,33]

To explain the multiple emission peaks in our spectra, we therefore invoke an effect that has not been observed in single-particle studies of colloidal quantum dots. PL from charged excitons can show multiple emission lines due to "shakeup". This process is a form of Auger coupling between two electrons in the conduction band and a hole in the valence band. One of the electrons recombines with the hole while the other "resident" electron is excited to a higher level in the conduction band. In contrast to Auger recombination, which is nonradiative because the resident electron accepts *all* of the recombination energy, the resident electron accepts only a fraction of the energy in the shakeup process. The remaining recombination energy is emitted as a photon. Depending on the conduction-band level to which the resident electron is excited, the photon energy can have multiple discrete values (Figure 3a). This would explain the observation of multiple emission peaks. Indeed, shakeup lines have previously been observed in epitaxial quantum wells.[44−46] For quantum dots in the strong confinement limit, these transitions are forbidden due to the orthogonality of the electron wave function of the trion and the excited single-electron wave functions.[47] However, in our case, these transitions are expected to be enabled by the weak lateral confinement of the charge carriers in the NPLs and the strong binding between the charge carriers in the trion, which modifies the wave functions. Potentially, shakeup emission could also be observed from negatively charged spherical quantum dots, e.g., those with a thick shell in which charge-carrier confinement is relaxed.
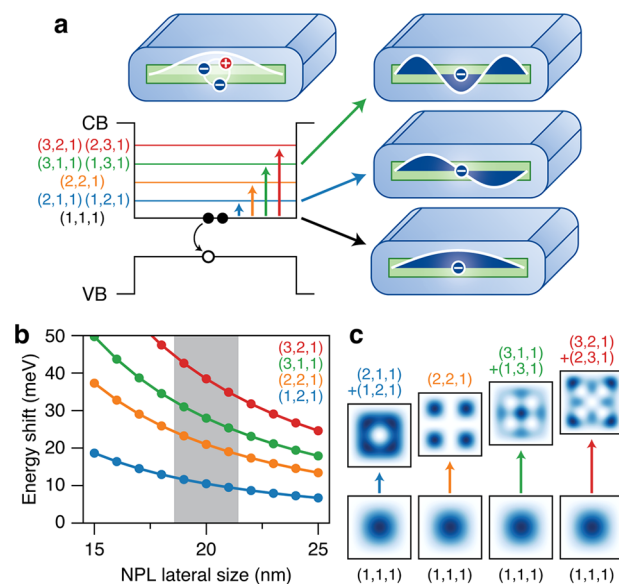

Figure 3. Electron shakeup in negatively charged core/shell NPLs. (a) When one of the electrons of the trion recombines with the hole in the valence band, the other electron can accept part of the recombination energy through Auger coupling. It can be excited into one of the many single-electron states of the NPL [indexed here by their quantum numbers (l, m, n)]. (b) Excited-state energies of a single electron in the particle-in-a-box model as a function of the CdSe NPL lateral size, with respect to the ground-state energy. The gray shaded area corresponds to the size estimated for our NPLs by transmission electron microscopy (TEM). (c) Electron probability density for the single-electron excited states and the corresponding shakeup transitions. The black square denotes the lateral extent of the NPL. For degenerate states, the electron probability densities of both states are combined.

To check if the peak energy differences observed in our experiments agree with the energies expected for electron shakeup, we calculated the energies of the excited states of a single electron in the conduction band. In the most simple approximation, the electron in the NPL can be modeled as a three-dimensional (3D) particle-in-a-box problem with an infinite potential barrier. Using the effective mass model[48−50] yields energies

$$E_{l,m,n} = \frac{\hbar^2 \pi^2}{2} \left(\frac{l^2}{m_{e,\parallel} L_x^2} + \frac{m^2}{m_{e,\parallel} L_y^2} + \frac{n^2}{m_{e,z} L_z^2} \right)$$

where l, m, and n and L_x, L_y, and L_z are the quantum numbers and dimensions of the NPL in the x, y, and z direction, respectively. For the in-plane ($m_{e,\parallel}$) and out-of-plane ($m_{e,z}$) effective masses, we took values from Rajadell et al.[51] Figure 3b shows the calculated energy differences between higher-excited states and the single-electron ground state. The relatively large NPL lateral dimensions of $L_x = L_y = 20$ nm lead to small energy differences of ~10 meV between levels. Figure 3c depicts the wave functions for the lowest-energy single-electron final states. For degenerate states, we have combined their electron probability densities. Comparing the calculated energy differences to the observed peak energy differences in Figure 2g,h, we see that the experimental data are indeed consistent with electron shakeup.

To investigate if the sudden switching of the emission lines of individual NPLs (Figure 1b) can also be explained by the shakeup model, the emission from the different clusters in
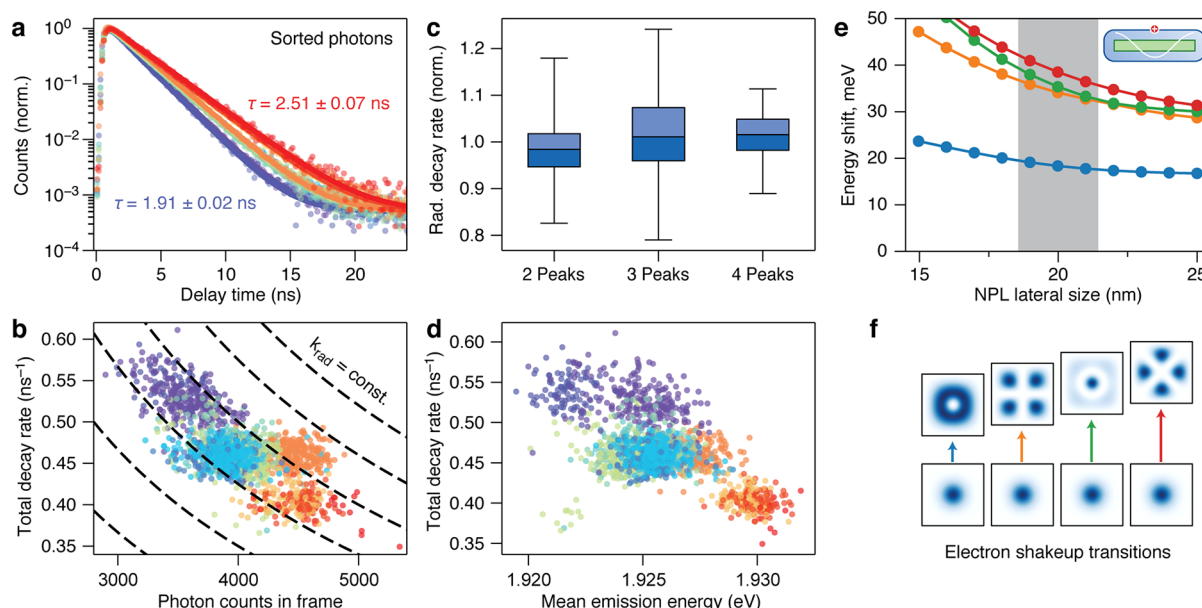
Figure 4. Time-dependent decay dynamics and the influence of spectator charges on the NPL surface. (a) Separate decay histograms for each cluster in Figure 2 (using the same color scheme). Solid lines are single-exponential fits with the same background level as in Figure 1d. The fitted values for the lifetime are explicitly written for the cluster with the fastest (purple) and slowest (red) decay. (b) For each frame, a single-exponential model was fit to the data with a maximum-likelihood estimator and the decay rate is plotted versus the total number of photons collected in the frame. The color of each data point shows which cluster the frame has been sorted into, and the dashed lines represent isolines of constant radiative decay rate. (c) Correlation between the number of emission peaks in the spectra and the normalized radiative decay rate, which we assume to scale linearly with the amplitude of the PL decay trace. The horizontal line inside the box indicates the median value, the box extends from the lower to upper quartile values of the data, and the whiskers highlight the span of the data points. (d) Correlation between the total decay rate and the mean emission energy. (e) Single-electron excited-state energies as a function of the NPL lateral size in the presence of a positive charge on the shell surface. (f) Probability density for the single-electron excited states and the corresponding shakeup transitions for the case with a positive charge on the NPL surface. The black square denotes the lateral extent of the NPL.

Figure 2b must be characterized in more detail. Consequently, we considered how the PL decay dynamics is correlated with the emission spectrum by sorting the photon arrival times by cluster. Figure 4a shows the extracted decay dynamics for each of the 12 different emission clusters. This analysis shows a small but clear variation in total excited-state lifetime of ~20−30% for the different clusters. To determine the relative contributions of radiative and nonradiative decay, we fit the decay trace of each individual frame using a maximum-likelihood estimation[52] procedure to the single-exponential decay function

$$\Phi(t) = A e^{-k_{tot}t}$$

where A is the amplitude and k_{tot} is the total decay rate of the NPL. Figure 4b shows the total decay rate k_{tot} of each frame versus the total number of photons N measured for each frame. These parameters should be related as

$$N = C\frac{k_{rad}}{k_{tot}}$$

where C is some constant that depends on the detection efficiency of our setup and the excitation power used and k_{rad} is the radiative decay rate of the NPL. Dashed lines in the plot correspond to isolines of constant radiative decay rate. While some variation (or fitting uncertainty) in the total decay rate exists, we observe that the data follow the trend of constant radiative decay rate. From this, we conclude that, as the NPL switches between different emission states, the radiative decay rate stays mostly constant while the nonradiative rate varies. Indeed, the extracted *radiative* decay rate is not correlated with

the number of observed emission peaks (Figure 4c). The *total* decay rate, however, shows a negative correlation with the mean photon emission energy (Figure 4d).

These trends can be explained by considering local fluctuations in the confinement potential of the charge carriers in the NPL. Such fluctuations can lead to changes in the emission state,[53] most prominently in gradual or sudden shifts in the spectrum (Figure 1b). Indeed, the rate of Auger coupling has been shown to depend very sensitively on changes to the confinement potential.[54] Auger coupling influences the appearance of shakeup emission lines as well as the nonradiative recombination. Hence, minor changes in the confinement potential can result in variations of the nonradiative decay rate (Figure 4a,b). Simultaneously, variations in the degree of electron shakeup should occur. More specifically, stronger Auger coupling would lead to faster nonradiative decay and more intense low-energy shakeup lines. This is exactly the correlation that we observe in Figure 4d (and consistent with Figure 2f).

Fluctuations in the confinement potential could be caused by structural dynamics on the NPL surface or the core/shell interface. In quantum dots and nanorods, surface charges, oxidation, or changes in ligand coverage are thought to be responsible for blinking and spectral diffusion.[55,56] We hypothesize that the same effects also play a role in our NPLs and can influence the trion recombination process. To consider this possibility, we calculated the single-electron excited-state energies (Figure 4e) and the corresponding wave functions (Figure 4f) for the case where a positive surface charge (trapped hole) is present on the outer CdS shell (see

section S4 in the Supporting Information for details of the model). We find that the weak potentials that are induced modify the energy differences between the shakeup lines in a range that is consistent with our experimental results (Figure 1b). Even small changes in the applied potentials can shift the single-electron energies by several millielectronvolts (compare Figures 3b and 4e). They also strongly affect the Auger coupling between confined charge carriers.[54]

We note that a surface charge rapidly moving between different surface sites by itself cannot explain the multiple emission peaks observed in Figure 1b. The spectra are sometimes constant for seconds with fixed relative peak intensities, which would imply that the surface charge switches between the different possible sites frequently within the integration time to suppress statistical fluctuations. When all of the emission peaks suddenly shift together, this would imply that all possible sites for the surface charge change simultaneously, which is unlikely.

Our discussion above suggests how the complex emission spectra of CdSe/CdS NPLs at cryogenic temperatures can be understood. A question that remains is whether this knowledge can be exploited to avoid the multiple emission features and obtain narrower emission from these materials, which extends to the ensemble level. A potential strategy to avoid shakeup replicas would be the synthesis of laterally small NPLs, which would bring them toward the strong-confinement limit in all three dimensions. In this case, shakeup transitions would be forbidden due to the orthogonality of the single-electron ground state and its excited states. However, the 3D strong confinement of the charge carriers would also result in strong sensitivity of the exciton (or trion) energies to small differences in the NPL lateral size, which would lead to undesirable inhomogeneous broadening if the lateral-size distribution cannot be controlled sufficiently. An alternative strategy for potentially suppressing shakeup replicas would be to use thinner CdS shells of only a few monolayers, rather than the ~12 monolayers present in our samples. Charges on the outer shell surface would then be closer to the active NPL core, leading to stronger induced charge-carrier confinement potentials. Local minima in the potential-energy landscape could then essentially create quantum dots within the 2D NPLs.[29] However, while the increased confinement would suppress shakeup emission, it would lead to even stronger dependence of the spectrum on the location of the surface charges. This would again result in more pronounced inhomogeneous broadening and stronger fluctuations of the spectrum of an individual NPL (compare Figure 1b). Thus, simple solutions may not exist to avoid broadening in CdSe/CdS core/shell NPLs due to the shakeup process at low temperature. However, controlling and reducing the level of charging of the NPLs may provide a possible route. By choosing suitable ligands or applying an electrochemical potential, charging of CdSe quantum dots has been suppressed.[57−59]

In summary, we report emission spectra from individual CdSe/CdS core/shell NPLs at cryogenic temperatures. We find an unexpectedly complex series of narrow peaks that change over time. We analyzed these NPL emission spectra and their corresponding photoluminescence decay dynamics using machine-learning algorithms with minimal user input. We attribute the observed peaks in the spectra to emission from negatively charged trions combined with a shakeup process. Upon electron−hole radiative recombination, the

extra electron in the trion is excited into one of several higher energy single-particle states. Mobile surface defects or surface charges strongly affect the coupling of the trion ground state to the different shakeup lines, therefore leading to broadening of the intrinsic ensemble line widths. Identifying strategies to suppress shakeup lines in core/shell nanoplatelets could therefore be an important step toward reducing line width broadening in these materials.

ASSOCIATED CONTENT

Ⓢ Supporting Information

The Supporting Information is available free of charge on the ACS Publications website at DOI: 10.1021/acs.nanolett.9b02856.

Detailed description of the sample fabrication, optical measurements, data analysis, and numerical models; table of parameter values used for the single-electron wave-function calculations; figures of the experimental setup, additional optical data, spectral sorting, histograms of peak energy differences, (PDF)

AUTHOR INFORMATION

Corresponding Author
*Email: dnorris@ethz.ch.

ORCID ⓘ
Felipe V. Antolinez: 0000-0002-1787-0112
Freddy T. Rabouw: 0000-0002-4775-0859
Aurelio A. Rossinelli: 0000-0001-6930-4190
David J. Norris: 0000-0002-3765-0678

Present Addresses
†Debye Institute for Nanomaterials Science, Utrecht University, Princetonplein 1, 3584 CC Utrecht, The Netherlands.
‡Helmholtz Zentrum München, Ingolstädter Landstrasse 1, 85764 Neuherberg, Germany.

REFERENCES

(1) Joo, J.; Son, J. S.; Kwon, S. G.; Yu, J. H.; Hyeon, T. Low-Temperature Solution-Phase Synthesis of Quantum Well Structured CdSe Nanoribbons. *J. Am. Chem. Soc.* **2006**, *128*, 5632−5633.

(2) Schliehe, C.; Juarez, B. H.; Pelletier, M.; Jander, S.; Greshnykh, D.; Nagel, M.; Meyer, A.; Foerster, S.; Kornowski, A.; Klinke, C.; Weller, H. Ultrathin PbS Sheets by Two-Dimensional Oriented Attachment. *Science* **2010**, *329*, 550−553.

(3) Liu, Y.-H.; Wang, F.; Wang, Y.; Gibbons, P. C.; Buhro, W. E. Lamellar Assembly of Cadmium Selenide Nanoclusters into Quantum Belts. *J. Am. Chem. Soc.* **2011**, *133*, 17005−17013.

(4) Ithurria, S.; Dubertret, B. Quasi 2D Colloidal CdSe Platelets with Thicknesses Controlled at the Atomic Level. *J. Am. Chem. Soc.* **2008**, *130*, 16504−16505.

(5) Ithurria, S.; Tessier, M. D.; Mahler, B.; Lobo, R. P. S. M.; Dubertret, B.; Efros, Al. L. Colloidal Nanoplatelets with Two-Dimensional Electronic Structure. *Nat. Mater.* **2011**, *10*, 936−941.

(6) Riedinger, A.; Ott, F. D.; Mule, A.; Mazzotti, S.; Knüsel, P. N.; Kress, S. J. P.; Prins, F.; Erwin, S. C.; Norris, D. J. An Intrinsic Growth Instability in Isotropic Materials Leads to Quasi-Two-Dimensional Nanoplatelets. *Nat. Mater.* **2017**, *16*, 743−749.

(7) Cho, W.; Kim, S.; Coropceanu, I.; Srivastava, V.; Diroll, B. T.; Hazarika, A.; Fedin, I.; Galli, G.; Schaller, R. D.; Talapin, D. V. Direct Synthesis of Six-Monolayer (1.9 nm) Thick Zinc-Blende CdSe Nanoplatelets Emitting at 585 nm. *Chem. Mater.* **2018**, *30*, 6957−6960.

(8) Christodoulou, S.; Climente, J. I.; Planelles, J.; Brescia, R.; Prato, M.; Martín-Garciá, B.; Khan, A. H.; Moreels, I. Chloride-Induced Thickness Control in CdSe Nanoplatelets. *Nano Lett.* **2018**, *18*, 6248−6254.

(9) Kumagai, M.; Takagahara, T. Excitonic and Nonlinear-Optical Properties of Dielectric Quantum-Well Structures. *Phys. Rev. B: Condens. Matter Mater. Phys.* **1989**, *40*, 12359−12381.

(10) Grim, J. Q.; Christodoulou, S.; Di Stasio, F.; Krahne, R.; Cingolani, R.; Manna, L.; Moreels, I. Continuous-Wave Biexciton Lasing at Room Temperature Using Solution-Processed Quantum Wells. *Nat. Nanotechnol.* **2014**, *9*, 891−895.

(11) Yang, Z.; Pelton, M.; Fedin, I.; Talapin, D. V.; Waks, E. A Room Temperature Continuous-Wave Nanolaser Using Colloidal Quantum Wells. *Nat. Commun.* **2017**, *8*, 143.

(12) Li, Q.; Liu, Q.; Schaller, R. D.; Lian, T. Reducing the Optical Gain Threshold in Two-Dimensional CdSe Nanoplatelets by the Giant Oscillator Strength Transition Effect. *J. Phys. Chem. Lett.* **2019**, *10*, 1624−1632.

(13) Tessier, M. D.; Javaux, C.; Maksimovic, I.; Loriette, V.; Dubertret, B. Spectroscopy of Single CdSe Nanoplatelets. *ACS Nano* **2012**, *6*, 6751−6758.

(14) Hines, M. A.; Guyot-Sionnest, P. Synthesis and Characterization of Strongly Luminescing ZnS-Capped CdSe Nanocrystals. *J. Phys. Chem.* **1996**, *100*, 468−471.

(15) Boldt, K.; Kirkwood, N.; Beane, G. A.; Mulvaney, P. Synthesis of Highly Luminescent and Photo-Stable, Graded Shell CdSe/Cd$_x$Zn$_{1-x}$S Nanoparticles by in Situ Alloying. *Chem. Mater.* **2013**, *25*, 4731−4738.

(16) Reiss, P.; Protière, M.; Li, L. Core/Shell Semiconductor Nanocrystals. *Small* **2009**, *5*, 154−168.

(17) Ithurria, S.; Talapin, D. V. Colloidal Atomic Layer Deposition (c-ALD) Using Self-Limiting Reactions at Nanocrystal Surface Coupled to Phase Transfer between Polar and Nonpolar Media. *J. Am. Chem. Soc.* **2012**, *134*, 18585−18590.

(18) Tessier, M. D.; Mahler, B.; Nadal, B.; Heuclin, H.; Pedetti, S.; Dubertret, B. Spectroscopy of Colloidal Semiconductor Core/Shell Nanoplatelets with High Quantum Yield. *Nano Lett.* **2013**, *13*, 3321−3328.

(19) Rossinelli, A. A.; Riedinger, A.; Marqués-Gallego, P.; Knüsel, P. N.; Antolinez, F. V.; Norris, D. J. High-Temperature Growth of Thick-Shell CdSe/CdS Core/Shell Nanoplatelets. *Chem. Commun.* **2017**, *53*, 9938−9941.

(20) Jianbo Shi; Malik, J. Normalized Cuts and Image Segmentation. *IEEE Trans. Pattern Anal. Mach. Intell.* **2000**, *22*, 888−905.

(21) Baldi, P.; Hatfield, G. W. *DNA Microarrays and Gene Expression*; Cambridge University Press: Cambridge, England, 2002.

(22) Efros, Al. L.; Nesbitt, D. J. Origin and Control of Blinking in Quantum Dots. *Nat. Nanotechnol.* **2016**, *11*, 661−671.

(23) Biadala, L.; Liu, F.; Tessier, M. D.; Yakovlev, D. R.; Dubertret, B.; Bayer, M. Recombination Dynamics of Band Edge Excitons in Quasi-Two-Dimensional CdSe Nanoplatelets. *Nano Lett.* **2014**, *14*, 1134−1139.

(24) Javaux, C.; Mahler, B.; Dubertret, B.; Shabaev, A.; Rodina, A. V.; Efros, Al. L.; Yakovlev, D. R.; Liu, F.; Bayer, M.; Camps, G.;

Biadala, L.; Buil, S.; Quelin, X.; Hermier, J.-P. Thermal Activation of Non-Radiative Auger Recombination in Charged Colloidal Nanocrystals. *Nat. Nanotechnol.* **2013**, *8*, 206−212.

(25) Gómez, D. E.; Van Embden, J.; Mulvaney, P.; Fernée, M. J.; Rubinsztein-Dunlop, H. Exciton-Trion Transitions in Single CdSe-CdS Core-Shell Nanocrystals. *ACS Nano* **2009**, *3*, 2281−2287.

(26) Dordević, N.; Beckwith, J. S.; Yarema, M.; Yarema, O.; Rosspeintner, A.; Yazdani, N.; Leuthold, J.; Vauthey, E.; Wood, V. Machine Learning for Analysis of Time-Resolved Luminescence Data. *ACS Photonics* **2018**, *5*, 4888−4895.

(27) Kanungo, T.; Mount, D. M.; Netanyahu, N. S.; Piatko, C. D.; Silverman, R.; Wu, A. Y. An Efficient K-Means Clustering Algorithm: Analysis and Implementation. *IEEE Trans. Pattern Anal. Mach. Intell.* **2002**, *24*, 881−892.

(28) Pedregosa, F.; Varoquaux, G.; Gramfort, A.; Michel, V.; Thirion, B.; Grisel, O.; Blondel, M.; Prettenhofer, P.; Weiss, R.; Dubourg, V.; Vanderplas, J.; Passos, A.; Cournapeau, D.; Brucher, M.; Perrot, M.; Duchesnay, E. Scikit-Learn: Machine Learning in Python. *J. Mach. Learn. Res.* **2011**, *12*, 2825−2830.

(29) Srivastava, A.; Sidler, M.; Allain, A. V.; Lembke, D. S.; Kis, A.; Imamoğlu, A. Optically Active Quantum Dots in Monolayer WSe$_2$. *Nat. Nanotechnol.* **2015**, *10*, 491−496.

(30) Fernée, M. J.; Tamarat, P.; Lounis, B. Cryogenic Single-Nanocrystal Spectroscopy: Reading the Spectral Fingerprint of Individual CdSe Quantum Dots. *J. Phys. Chem. Lett.* **2013**, *4*, 609−618.

(31) Fernée, M. J.; Littleton, B. N.; Rubinsztein-Dunlop, H. Detection of Bright Trion States Using the Fine Structure Emission of Single CdSe/ZnS Colloidal Quantum Dots. *ACS Nano* **2009**, *3*, 3762−3768.

(32) Louyer, Y.; Biadala, L.; Trebbia, J. B.; Fernée, M. J.; Tamarat, P.; Lounis, B. Efficient Biexciton Emission in Elongated Cdse/ZnsCdSe/ZnS Nanocrystals. *Nano Lett.* **2011**, *11*, 4370−4375.

(33) Shornikova, E. V.; Biadala, L.; Yakovlev, D. R.; Sapega, V. F.; Kusrayev, Y. G.; Mitioglu, A. A.; Ballottin, M. V.; Christianen, P. C. M.; Belykh, V. V.; Kochiev, M. V.; et al. Addressing the Exciton Fine Structure in Colloidal Nanocrystals: The Case of CdSe Nanoplatelets. *Nanoscale* **2018**, *10*, 646−656.

(34) Park, Y. S.; Bae, W. K.; Pietryga, J. M.; Klimov, V. I. Auger Recombination of Biexcitons and Negative and Positive Trions in Individual Quantum Dots. *ACS Nano* **2014**, *8*, 7288−7296.

(35) Kunneman, L. T.; Tessier, M. D.; Heuclin, H.; Dubertret, B.; Aulin, Y. V.; Grozema, F. C.; Schins, J. M.; Siebbeles, L. D. A. Bimolecular Auger Recombination of Electron−Hole Pairs in Two-Dimensional CdSe and CdSe/CdZnS Core/Shell Nanoplatelets. *J. Phys. Chem. Lett.* **2013**, *4*, 3574−3578.

(36) Nirmal, M.; Norris, D. J.; Kuno, M.; Bawendi, M. G.; Efros, Al. L.; Rosen, M. Observation of the "Dark Exciton" in CdSe Quantum Dots. *Phys. Rev. Lett.* **1995**, *75*, 3728−3731.

(37) Fernée, M. J.; Tamarat, P.; Lounis, B. Spectroscopy of Single Nanocrystals. *Chem. Soc. Rev.* **2014**, *43*, 1311−1337.

(38) Beyler, A. P.; Marshall, L. F.; Cui, J.; Brokmann, X.; Bawendi, M. G. Direct Observation of Rapid Discrete Spectral Dynamics in Single Colloidal CdSe-CdS Core-Shell Quantum Dots. *Phys. Rev. Lett.* **2013**, *111*, 177401.

(39) Lorenzon, M.; Christodoulou, S.; Vaccaro, G.; Pedrini, J.; Meinardi, F.; Moreels, I.; Brovelli, S. Reversed Oxygen Sensing Using Colloidal Quantum Wells towards Highly Emissive Photoresponsive Varnishes. *Nat. Commun.* **2015**, *6*, 6434.

(40) Klimov, V.; Bolivar, P. H.; Kurz, H. Ultrafast Carrier Dynamics in Semiconductor Quantum Dots. *Phys. Rev. B: Condens. Matter Mater. Phys.* **1996**, *53*, 1463−1467.

(41) Jones, M.; Lo, S. S.; Scholes, G. D. Quantitative Modeling of the Role of Surface Traps in CdSe/CdS/ZnS Nanocrystal Photoluminescence Decay Dynamics. *Proc. Natl. Acad. Sci. U. S. A.* **2009**, *106*, 3011−3016.

(42) Utterback, J. K.; Grennell, A. N.; Wilker, M. B.; Pearce, O. M.; Eaves, J. D.; Dukovic, G. Observation of Trapped-Hole Diffusion on the Surfaces of CdS Nanorods. *Nat. Chem.* **2016**, *8*, 1061−1066.

(43) Kunneman, L. T.; Schins, J. M.; Pedetti, S.; Heuclin, H.; Grozema, F. C.; Houtepen, A. J.; Dubertret, B.; Siebbeles, L. D. A. Nature and Decay Pathways of Photoexcited States in CdSe and CdSe/CdS Nanoplatelets. *Nano Lett.* **2014**, *14*, 7039−7045.

(44) Nash, K. J.; Skolnick, M. S.; Saker, M. K.; Bass, S. J. Many Body Shakeup in Quantum Well Luminescence Spectra. *Phys. Rev. Lett.* **1993**, *70*, 3115−3118.

(45) Finkelstein, G.; Shtrikman, H.; Bar-Joseph, I. Shakeup Processes in the Recombination Spectra of Negatively Charged Excitons. *Phys. Rev. B: Condens. Matter Mater. Phys.* **1996**, *53*, 12593−12596.

(46) Paskov, P. P.; Holtz, P. O.; Wongmanerod, S.; Monemar, B.; Garcia, J. M.; Schoenfeld, W. V.; Petroo, P. M. Auger Processes in InAs Self-Assembled Quantum Dots. *Phys. E* **2000**, *6*, 440−443.

(47) Efros, Al. L. Personal communication.

(48) Griffiths, D. J. *Introduction to Quantum Mechanics*; Pearson Education: Upper Saddle River, NJ, 2005.

(49) Gotoh, H.; Ando, H.; Takagahara, T. Radiative Recombination Lifetime of Excitons in Thin Quantum Boxes. *J. Appl. Phys.* **1997**, *81*, 1785−1789.

(50) Benchamekh, R.; Gippius, N. A.; Even, J.; Nestoklon, M. O.; Jancu, J. M.; Ithurria, S.; Dubertret, B.; Efros, Al. L.; Voisin, P. Tight-Binding Calculations of Image-Charge Effects in Colloidal Nanoscale Platelets of CdSe. *Phys. Rev. B: Condens. Matter Mater. Phys.* **2014**, *89*, 035307.

(51) Rajadell, F.; Climente, J. I.; Planelles, J. Excitons in Core-Only, Core-Shell and Core-Crown CdSe Nanoplatelets: Interplay between in-Plane Electron-Hole Correlation, Spatial Confinement, and Dielectric Confinement. *Phys. Rev. B: Condens. Matter Mater. Phys.* **2017**, *96*, 035307.

(52) Bajzer, Z.; Therneau, T. M.; Sharp, J. C.; Prendergast, F. G. Maximum Likelihood Method for the Analysis of Time-Resolved Fluorescence Decay Curves. *Eur. Biophys. J.* **1991**, *20*, 247−262.

(53) Empedocles, S. A.; Bawendi, M. G. Quantum-Confined Stark Effect in Single CdSe Nanocrystallite Quantum Dots. *Science* **1997**, *278*, 2114−2117.

(54) Cragg, G. E.; Efros, Al. L. Suppression of Auger Processes in Confined Structures. *Nano Lett.* **2010**, *10*, 313−317.

(55) Empedocles, S. A.; Norris, D. J.; Bawendi, M. G. Photoluminescence Spectroscopy of Single CdSe Nanocrystallite Quantum Dots. *Phys. Rev. Lett.* **1996**, *77*, 3873−3876.

(56) Lohmann, S. H.; Strelow, C.; Mews, A.; Kipp, T. Surface Charges on CdSe-Dot/CdS-Rod Nanocrystals: Measuring and Modeling the Diffusion of Exciton-Fluorescence Rates and Energies. *ACS Nano* **2017**, *11*, 12185−12192.

(57) Hohng, S.; Ha, T. Near-Complete Suppression of Quantum Dot Blinking in Ambient Conditions. *J. Am. Chem. Soc.* **2004**, *126*, 1324−1325.

(58) Jha, P. P.; Guyot-Sionnest, P. Trion Decay in Colloidal Quantum Dots. *ACS Nano* **2009**, *3*, 1011−1015.

(59) Galland, C.; Ghosh, Y.; Steinbrück, A.; Sykora, M.; Hollingsworth, J. A.; Klimov, V. I.; Htoon, H. Two Types of Luminescence Blinking Revealed by Spectroelectrochemistry of Single Quantum Dots. *Nature* **2011**, *479*, 203−207.

■ NOTE ADDED AFTER ASAP PUBLICATION

This paper was published ASAP on November 13, 2019 with an incomplete Supporting Information file. The new file was uploaded and the paper reposted on November 15, 2019.